Computers and Structures 89 (2011) 2471–2483

Contents lists available at ScienceDirect

Computers and Structures

journal homepage: www.elsevier.com/locate/compstruc

Dynamic analysis of tensegrity structures using a complementarity framework

N.D. Oliveto [a,1], M.V. Sivaselvan [b,*]

[a] Department of Civil, Structural and Environmental Engineering, University at Buffalo, 225 Ketter Hall, Buffalo, NY 14260, USA
[b] Department of Civil, Environmental and Architectural Engineering, University of Colorado at Boulder, 428 UCB, Boulder, CO 80309, USA

ARTICLE INFO

Article history:
Received 12 November 2010
Accepted 15 June 2011
Available online 12 July 2011

Keywords:
Tensegrity
Complementarity
Dynamic analysis
Energy balance

ABSTRACT

An approach is presented for dynamic analysis of tensegrity structures in the small displacement regime. Such analyses are characterized by cables switching between taut and slack states. The approach is based on casting the computation in each time increment as a complementarity problem. Numerical examples are presented to illustrate the approach. Despite the nonsmooth nature of cables switching between taut and slack states, the computed solutions exhibit remarkable long-term energy balance. Furthermore, by exploiting some features of the tensegrity model, significant computational efficiency can be gained in the solution of the complementarity problem in each time increment. Due to the use of linearized kinematics, the method is not applicable as is to tensegrity structures with internal mechanisms or where the geometric stiffness is significant compared to the material stiffness. The method however plays a role in a more general nonlinear kinematics formulation.

1. Introduction

Tensegrity structures are a subclass of pin-jointed structures composed of cables or strings, which can only resist tension forces, and bars or struts that are mainly meant to work in compression. To minimize weight, it is desirable in engineering applications to limit the number of stocky bars as compared to the number of the relatively light cables. Stability under external loading is then achieved by pretension of those cables that would otherwise become slack. One of the main requirements for a structure to be categorized as a tensegrity structure is that its initial prestressed configuration must be in stable equilibrium in absence of external forces. The evaluation of such configurations, known as form-finding, has been and is currently object of extensive research [1]. A large body of literature is devoted to the topic, including recent applications using dynamic relaxation methods [2] and evolutionary strategies [3]. Besides the original interest in the field of civil engineering applications, which started developing with work by Calladine and Pellegrino [4,5], recent years have seen a multidisciplinary interest in tensegrity structures research [6], with these emerging as the structural systems of the future. Control, folding and deploying capabilities have inspired aerospace engineering applications concerning for instance space telescopes, flight simulators and antennas, [7–9]. Several applications are appearing in the field of biomedical engineering [10–12], where cell, tissue and organ architecture seem to adhere to models similar to those describing the behavior of tensegrity structures. Some applications have appeared also in the field of robotics where the characteristics of tensegrity structures make them appealing candidates for the design of movable robots as well as for manipulators [13–15]. One interesting and promising aspect of tensegrity structures, which to our knowledge has not yet been developed much in the literature, is their potential ability to control the response to seismic excitations. A detailed discussion of tensegrity structures including historical background, analysis, design and control can be found in [16]. We also refer the reader to the survey articles [17,18] on static and dynamic analysis of tensegrity structures.

The objective of this paper is to present an approach for the dynamic analysis of tensegrity structures in the small displacement regime. The novelty of the approach lies in casting the computations that occur in each time increment of the dynamic analysis as a "complementarity" problem. This formulation is made possible by the following fact. For any cable, the force in the cable and the slack are both non-negative, and when the force is positive, the slack is zero, and viceversa. The remarkable feature of the resulting approach is that despite the nonsmooth nature of cables switching between taut and slack states, the computed solutions show excellent long-term energy balance. Nineb et.al. [19] have used a complementarity framework in the context of a domain decomposition approach for nonsmooth problems, specifically tensegrity structures. We discuss the relation of the formulation

* Corresponding author.
E-mail addresses: noliveto@buffalo.edu (N.D. Oliveto), siva@colorado.edu (M.V. Sivaselvan).
[1] Visiting Scholar, University of Colorado at Boulder.

0045-7949/$ - see front matter © 2011 Elsevier Ltd. All rights reserved.
doi:10.1016/j.compstruc.2011.06.003

Nomenclature

A_b	area of bars in Examples 1 and 2
A_c	area of cables in Examples 1 and 2
$\mathbf{A}_c$	diagonal matrix of elastic compliances in tension of all cables in the structure
$\mathbf{b}$, $\mathbf{b}_1$, $\mathbf{b}_2$	see Eq. (7b)
$\mathbf{B}_b$	matrix that relates the node displacements to bar deformations
$\mathbf{B}_c$	matrix that relates the node displacements to cable deformations
$\mathbf{b}_{\text{UNI}}$	vector associated with unilateral constraints appearing in Eq. (4); for tension-only behavior $\mathbf{b}_{\text{UNI}} = 0$
$\mathbf{C}$	matrix representing inherent damping in the structure
E_b	Young's modulus of bars in Examples 1 and 2
E_c	Young's modulus of cables in Examples 1 and 2
F	force in a cable
f_{1-6}	frequencies of the first 6 modes of the linearized model in Example 2
$\mathbf{f}_0^b$	vector of prestress forces in bars
$\mathbf{f}^c$	vector of forces in the cables
$\tilde{\mathbf{f}}_n^c$	vector of predictor forces in cables (Eq. (6))
g	acceleration due to gravity
H	height of tensegrity module in Examples 1 and 2
h	time increment
$\mathbf{K}_b^{\text{global}}$	part of the structure stiffness matrix arising from the bars
$\mathbf{K}_c$	diagonal matrix of elastic stiffnesses in tension of all cables in the structure ($\mathbf{K}_c = \mathbf{A}_c^{-1}$)
$\mathbf{K}^{\text{global}}$	elastic global stiffness matrix including the contributions of the bars and cables $= \mathbf{K}_b^{\text{global}} + \mathbf{B}_c^T \mathbf{K}_c \mathbf{B}_c$
L	length of tensegrity module in Examples 1 and 2
$\overline{\mathbf{M}}$	$\mathbf{M} + \frac{h}{2}\mathbf{C} + \frac{h^2}{4}\mathbf{K}^{\text{global}}$
$\mathcal{M}$	MCP matrix (see Eq. (8))
$\mathbf{M}$	mass matrix of the structure
n	time increment index
p	load on each node in Example 1
$\mathbf{p}$	vector of external nodal forces
$\mathbf{q}$	MCP vector (see Eq. (9))
R_s	support reaction used in computing input energy in the forced vibration analysis in Example 2
t	time
$\mathbf{u}$	vector of displacements at the free DOF of the structure
$\ddot{u}_g$	input base acceleration in Example 2
$\ddot{u}_{g0}$	amplitude of input base acceleration in Example 2
$\mathbf{v}$	vector of velocities at the free DOF of the structure
v_s	support velocity used in computing input energy in the forced vibration analysis in Example 2
$\mathbf{w}$	variable in the complementarity problem (10)
α	load factor in Example 1
Δ_0^c	vector of prestress deformations in cables
π	slack in a cable
$\boldsymbol{\pi}$	vector of slacks in the cables
$\boldsymbol{\Psi}_{\text{UNI}}$	matrix associated with unilateral constraints appearing in Eq. (4); for tension-only behavior $\boldsymbol{\Psi}_{\text{UNI}} = -\text{Identity}$
τ	dummy variable in the integral for the input energy in the forced vibration analysis in Example 2

presented here to that of Nineb et.al. [19] at the end of Section 4.1. The approach presented here builds on previous work on the application of complementarity formulations to elasto-plastic problems (for example [20,21]).

The organization of the paper is as follows. In Section 2, the modeling of tensegrity structures adopted here is discussed, resulting in a differential–algebraic system with complementarity conditions. This system is discretized in time in Section 3, leading to a complementarity problem in Section 4. Numerical examples are then presented in Section 5, highlighting the long-term energy balance in the solutions, and the computational efficiency gained by using some features of the model in solving the complementarity problem.

2. Modeling for dynamic analysis

We think of a tensegrity structure as a truss with two types of members – "bars" that are capable of acting in both tension and compression (although they are predominantly in compression), and "cables" that act in tension only (they develop slack otherwise). Each cable can be represented conceptually as shown in Fig. 1. Compatibility of deformations in this model of a cable implies

$$aF(t) - \pi(t) - \Delta(t) = 0 \tag{1}$$

where as shown in Fig. 1, a is the elastic compliance of the cable in tension, $F(t)$ is the force in the cable at time t, $\Delta(t)$ is the deformation, and $\pi(t)$ is the slack in the cable. The force in the cable and the slack are nonnegative. Furthermore, when the force in the cable is positive the slack is zero, and viceversa. This is expressed concisely by the "complementarity" conditions

$$F(t) \geqslant 0, \quad \pi(t) \geqslant 0, \quad F(t)\pi(t) = 0 \tag{2}$$

In the following, we consider only linearized kinematics (small displacements). Then the equation of motion of the structure, together

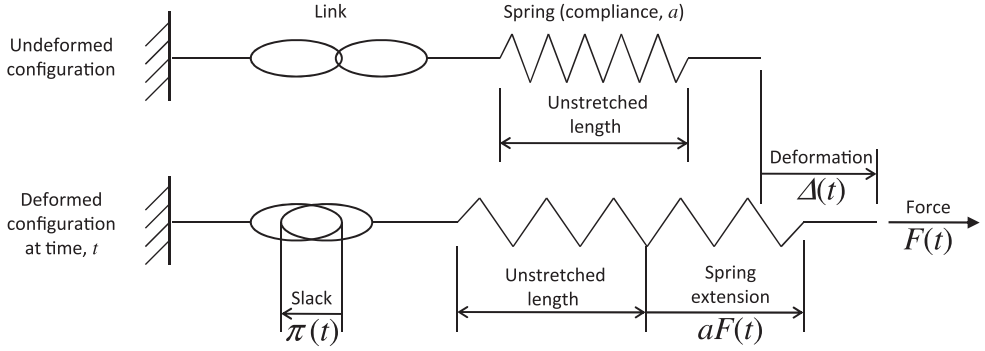

Fig. 1. Conceptual model of a cable in a tensegrity structure.

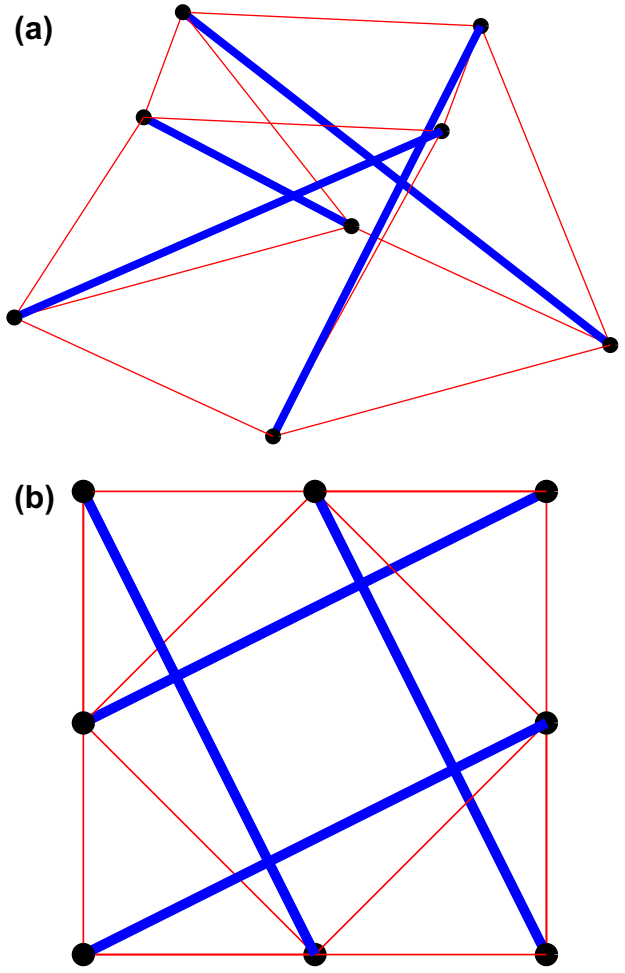

Fig. 2. Example 1 – Single module in the tensegrity structure (a) Isometric view (b) Plan view. (Cables are shown as thin (red) lines and bars as thick (blue) lines. This individual module has an internal mechanism, but as mentioned in Section 2.1 the assembled tensegrity grid does not.) (For interpretation of the references to colour in this figure legend, the reader is referred to the web version of this article.)

Table 1
Example 1 – Summary of module parameters.

Parameter	Value
Module height H	0.5 m
Module length L	1 m
Cross section of cables A_c	0.5×10^{-4} m^2
Young's modulus of cables E_c	10^{11} N/m^2
Cross section of bars A_b	2.8×10^{-4} m^2
Young's modulus of bars E_b	2×10^{11} N/m^2
Prestress in lower cables	2000 N
Prestress in upper cables	$2000\sqrt{2}$ N = 2828.4271 N
Prestress in bracing cables	$2000\sqrt{1+4(H/L)^2}$ N = 2828.4271 N
Prestress in bars	$-2000\sqrt{5+4(H/L)^2}$ N=-4898.9795 N

with collecting Eqs. (1) and (2) for all the cables in the structure, results in

$$\begin{aligned} &\mathbf{M}\ddot{\mathbf{u}}(t) + \mathbf{C}\dot{\mathbf{u}}(t) + \mathbf{K}_b^{\text{global}}\mathbf{u}(t) + \mathbf{B}_c^T\mathbf{f}^c(t) = \mathbf{p}(t) - \mathbf{B}_b^T\mathbf{f}_0^b \\ &\mathbf{A}_c\mathbf{f}^c(t) - \boldsymbol{\pi}(t) - \mathbf{B}_c\mathbf{u}(t) - \Delta_0^c = 0 \\ &\mathbf{f}^c(t) \geqslant 0, \boldsymbol{\pi}(t) \geqslant 0, \mathbf{f}^c(t)^T\boldsymbol{\pi}(t) = 0 \end{aligned} \tag{3}$$

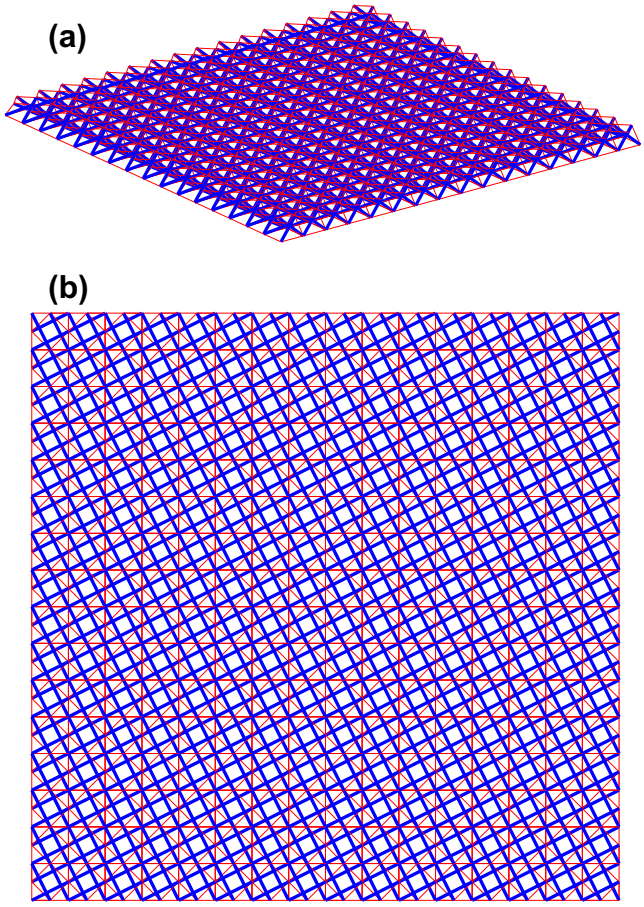

Fig. 3. Example 1 – Undeformed configuration. (a) Isometric view. (b) Plan view. (Cables are shown in thin red and bars in thick blue.) (For interpretation of the references to colour in this figure legend, the reader is referred to the web version of this article.)

where $\mathbf{M}$ is the mass matrix of the structure (a lumped or consistent mass matrix may be used), $\mathbf{C}$ is a matrix representing inherent damping in the structure, $\mathbf{K}_b^{\text{global}}$ is the part of the structure stiffness matrix arising from the bars, $\mathbf{u}$ is the vector of displacements at the free degrees of freedom (DOF) of the structure, $\mathbf{p}$ is the vector of external nodal forces, $\mathbf{A}_c$ is the diagonal matrix of elastic compliances in tension of all cables in the structure, $\mathbf{B}_c$ and $\mathbf{B}_b$ are the matrices that relate the node displacements to cable deformations and bar deformations respectively, $\mathbf{f}^c$ and $\boldsymbol{\pi}$ are the vectors of forces and slacks respectively in the cables, $\mathbf{f}_0^b$ is the vector of prestress forces in the bars, and Δ_0^c is the vector of prestress deformations in the cables. Dissipation associated with cables slackening and tightening can also be modeled. Modeling various dissipative mechanisms within the complementarity framework used here is discussed in reference [20].

Eq. (3) represents a linear differential–algebraic system with complementarity conditions. Due to the presence of the complementarity conditions, it represents nonsmooth dynamics. In this paper, we do not consider theoretical questions such as the existence and uniqueness of solutions to this system. The reader is referred to [22] for an exposition of such issues. Here, we take a heuristic approach. We formally discretize Eq. (3) in time, and consider the convergence of the resulting solutions with decreasing time increment.

Before discretizing the system (3), we cast it into a more general format as follows.

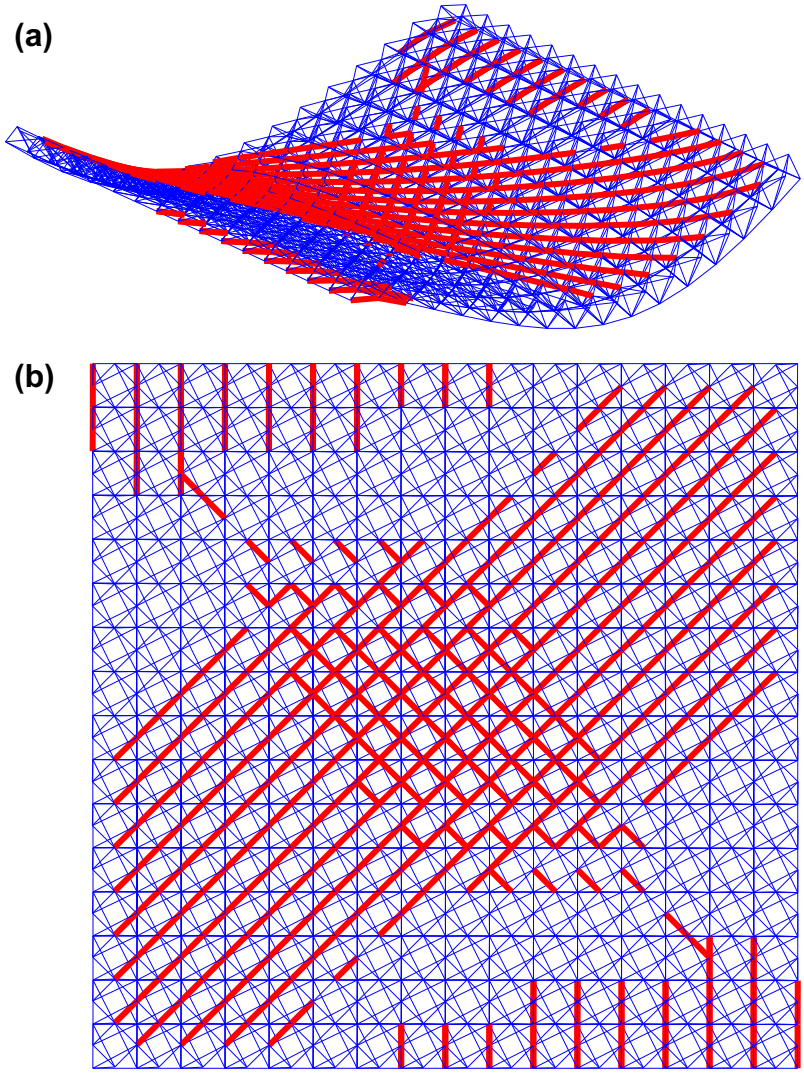

Fig. 4. Example 1 – Deformed configuration for $\alpha = 1$ with slack cables shown in thick (red) lines. (a) Isometric view. (b) Plan view. (For interpretation of the references to colour in this figure legend, the reader is referred to the web version of this article.)

$$\begin{aligned}
&\mathbf{M}\ddot{\mathbf{u}}(t) + \mathbf{C}\dot{\mathbf{u}}(t) + \mathbf{K}_b^{\text{global}}\mathbf{u}(t) + \mathbf{B}_c^T\mathbf{f}^c(t) = \mathbf{p}(t) - \mathbf{B}_b^T\mathbf{f}_0^b \\
&\mathbf{A}_c\mathbf{f}^c(t) + \boldsymbol{\Psi}_{\text{UNI}}^T\boldsymbol{\pi}(t) - \mathbf{B}_c\mathbf{u}(t) - \boldsymbol{\Delta}_0^c = 0 \\
&\boldsymbol{\Psi}_{\text{UNI}}\mathbf{f}^c(t) \leqslant \mathbf{b}_{\text{UNI}}, \quad \boldsymbol{\pi}(t) \geqslant 0, \quad \left(\mathbf{b}_{\text{UNI}} - \boldsymbol{\Psi}_{\text{UNI}}\mathbf{f}^c(t)\right)^T\boldsymbol{\pi}(t) = 0
\end{aligned} \tag{4}$$

where the subscript UNI stands for "unilateral constraints". The purpose of this generalization is twofold – (a) to allow for slightly more general behavior than tension-only (for example compression-only, interaction between force components etc.), (b) to align the notation with reference [20] where similar formulations result when modeling the dynamics of systems with softening plasticity. Eq. (3) are recovered from Eq. (4) by setting $\boldsymbol{\Psi}_{\text{UNI}} = -\text{Identity}$ and $\mathbf{b}_{\text{UNI}} = 0$. Before considering the time-discretization of this system in Section 3, we point out some consequences of the small-displacement assumption.

2.1. Implications of linearized kinematics

The use of linearized kinematics (small displacements) has some particular implications for tensegrity structures.

1. *Internal mechanisms*: If the equilibrium matrix $[\mathbf{B}_b\,\mathbf{B}_c]^T$ is not full rank, then the tensegrity structure has internal mechanisms. This is a common occurrence in tensegrity structures. The concept of internal mechanisms is explained in references [5,23] using the four fundamental subspaces of the equilibrium matrix, a basic idea in linear algebra. Such internal mechanisms cannot be stabilized within the context of linearized kinematics. Pellegrino and Calladine [24,25] present conditions under which these mechanisms can be stabilized by first order changes in the equilibrium matrix, which in turn are second order changes in the node displacement-member elongation relationship.
2. *Geometric stiffness*: Tensegrity structures are by definition pre-stressed frameworks, and carry non-zero internal forces in the reference configuration. Therefore, the effect of geometric stiffness could be significant even in the reference configuration. Geometric stiffness represents a first order change in the equilibrium matrix (see for example, [26]), i.e., a second order change in the node displacement-member elongation kinematics.

It is clear that with linearized kinematics, tensegrity structures structures with internal mechanisms or significant geometric

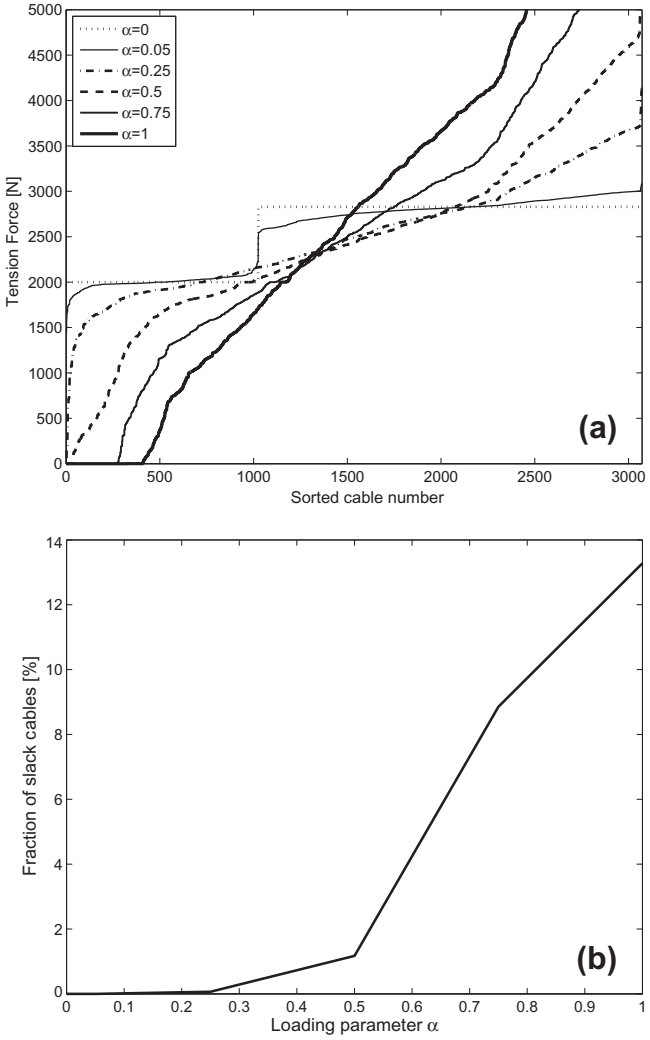

Fig. 5. Example 1 – (a) Cable tensions, and (b) fractions of slack cables, for different values of the load factor α (these computational results are identical to the respective results in reference [19]).

Table 2
Example 1 – Options for the PATH solver to imitate Lemke's method.

Option	Value
`crash_method`	`none`
`major_iteration_limit`	`1`
`lemke_start`	`always`
`output_minor_iteration_frequency`	`1`

stiffness effects cannot be analyzed. Therefore, the formulation presented here cannot be applied to such situations as is.

However, a formulation very similar to that presented here can be used to describe more general nonlinear kinematics, and therefore apply to the large displacement regime and to situations with internal mechanisms and significant geometric stiffness. In that case, due to the nonlinear relationship between member elongations and node displacements, and to the dependence of the equilibrium matrix on the configuration, a Newton-type algorithm would have to be used in each time increment. The exact strategy described in Section 4 of the manuscript (Eqs. (8)–(10)) would then apply to each iteration of such a Newton-type algorithm. The approach presented in this paper is therefore relevant in the large displacement regime as well. The large-displacement formulation is a topic of current work.

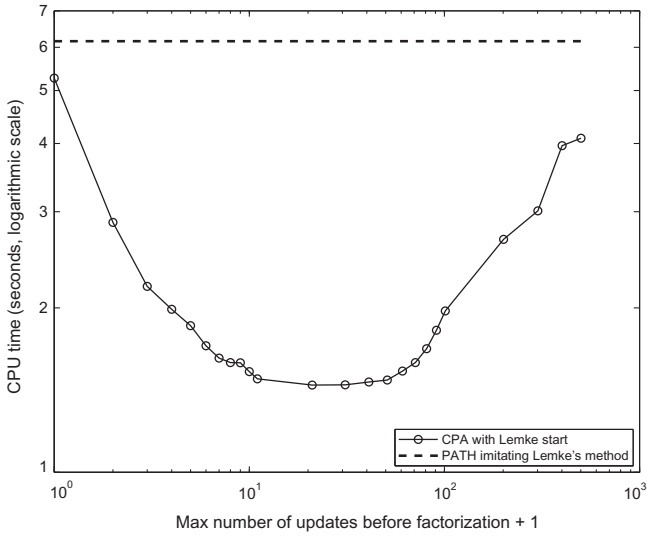

Fig. 6. Example 1 – Computational time (In this example, there are 2397 free DOF and 3072 cables, so that the size of the MCP in Eq. (10) is 5469).

Table 3
Example 2 – Summary of module parameters.

Parameter	Value
Module height H	1.15 m
Module length L	1.5 m
Cross section of cables A_c	0.654×10^{-4} m^2
Young's modulus of cables E_c	1.25×10^{11} N/m^2
Cross section of bars A_b	4.14×10^{-4} m^2
Young modulus of bars E_b	2×10^{11} N/m^2
Prestress in bars	−20000 N
Prestress in peripheral lower cables	7376.5536 N
Prestress in internal lower cables	14753.1072 N
Prestress in upper cables	10432.0221 N
Prestress in bracing cables	13503.5487 N

The numerical examples in this paper have been chosen such that the equilibrium matrices are full rank (so that there are no internal mechanisms), and the geometric stiffness is small compared to the material stiffness. It also turns out that internal mechanisms are not formed due to cables slackening during the analysis.

3. Time discretization

We discretize the system (4) formally as follows (see also references [27,28,20])

$$\begin{aligned}
&\mathbf{M}\left(\tfrac{\mathbf{v}_{n+1}-\mathbf{v}_n}{h}\right)+\mathbf{C}\left(\tfrac{\mathbf{v}_{n+1}+\mathbf{v}_n}{2}\right)+\mathbf{K}_b^{\text{global}}\left(\mathbf{u}_n+\tfrac{\mathbf{v}_{n+1}+\mathbf{v}_n}{4}h\right)\\
&\qquad+\mathbf{B}_c^T\left(\tfrac{\mathbf{f}_{n+1}^c+\mathbf{f}_n^c}{2}\right)=\tfrac{\mathbf{p}_{n+1}+\mathbf{p}_n}{2}-\mathbf{B}_b^T\mathbf{f}_0^b\\
&\mathbf{A}_c(\mathbf{f}_{n+1}^c-\mathbf{f}_n^c)+\boldsymbol{\Psi}_{\text{UNI}}^T(\boldsymbol{\pi}_{n+1}-\boldsymbol{\pi}_n)-\mathbf{B}_c\tfrac{\mathbf{v}_{n+1}+\mathbf{v}_n}{2}h=\mathbf{0}\\
&\boldsymbol{\Psi}_{\text{UNI}}\mathbf{f}_{n+1}^c\leqslant\mathbf{b}_{\text{UNI}},\boldsymbol{\pi}_{n+1}\geqslant 0,\quad\left(\mathbf{b}_{\text{UNI}}-\boldsymbol{\Psi}_{\text{UNI}}\mathbf{f}_{n+1}^c\right)^T\boldsymbol{\pi}_{n+1}=0
\end{aligned}\tag{5}$$

where h is the time increment, $\mathbf{v}$ is the vector of velocities at the free DOF, and the subscripts n and $n+1$ denote discrete times. When no cables are slack, this discretization reduces to the constant average acceleration version of Newmark's method (see for example [29]). The second of Eq. (5) can be written in the following predictor–corrector form.

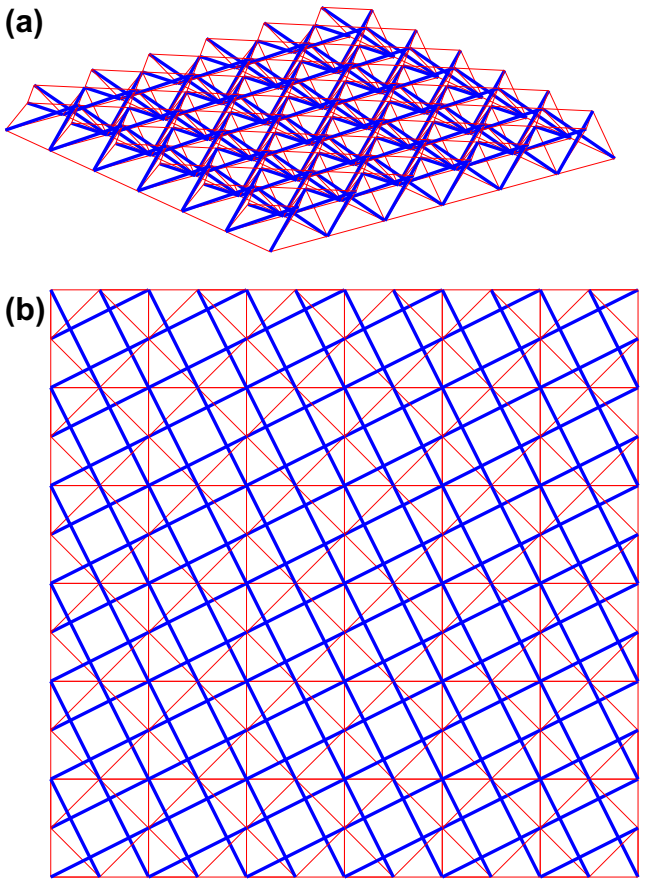

Fig. 7. Example 2 – Undeformed configuration. (a) Isometric view. (b) Plan view (cables are shown in thin red and bars in thick blue). (For interpretation of the references to colour in this figure legend, the reader is referred to the web version of this article.)

$$\begin{aligned}&\text{Predictor}: \tilde{\mathbf{f}}_n^c = \mathbf{f}_n^c + \mathbf{K}_c\left(\tfrac{h}{2}\mathbf{B}_c\mathbf{v}_n + \boldsymbol{\Psi}_{\text{UNI}}^T\boldsymbol{\pi}_n\right)\\ &\text{Corrector}: \mathbf{f}_{n+1}^c = \tilde{\mathbf{f}}_n^c + \mathbf{K}_c\left(\tfrac{h}{2}\mathbf{B}_c\mathbf{v}_{n+1} - \boldsymbol{\Psi}_{\text{UNI}}^T\boldsymbol{\pi}_{n+1}\right)\end{aligned} \tag{6}$$

where $\mathbf{K}_c$ is the diagonal matrix of elastic stiffnesses in tension of all cables in the structure ($\mathbf{K}_c = \mathbf{A}_c^{-1}$). Substituting the corrector equation into the first of Eq. (5), and into the inequality $\boldsymbol{\Psi}_{\text{UNI}}\mathbf{f}_{n+1}^c \leqslant \mathbf{b}_{\text{UNI}}$ gives

$$\begin{aligned}&\overline{\mathbf{M}}\mathbf{v}_{n+1} - \tfrac{h}{2}\mathbf{B}_c^T\mathbf{K}_c\boldsymbol{\Psi}_{\text{UNI}}^T\boldsymbol{\pi}_{n+1} = \mathbf{b}_1\\ &-\tfrac{h}{2}\boldsymbol{\Psi}_{\text{UNI}}\mathbf{K}_c\mathbf{B}_c\mathbf{v}_{n+1} + \boldsymbol{\Psi}_{\text{UNI}}\mathbf{K}_c\boldsymbol{\Psi}_{\text{UNI}}^T\boldsymbol{\pi}_{n+1} \geqslant \mathbf{b}_2\end{aligned} \tag{7a}$$

where $\overline{\mathbf{M}} = \mathbf{M} + \frac{h}{2}\mathbf{C} + \frac{h^2}{4}\mathbf{K}^{\text{global}}$ with $\mathbf{K}^{\text{global}} = \mathbf{K}_b^{\text{global}} + \mathbf{B}_c^T\mathbf{K}_c\mathbf{B}_c$, the elastic global stiffness matrix including the contributions of the bars and cables, and

$$\begin{aligned}\mathbf{b}_1 &= \tfrac{h}{2}\left[(\mathbf{p}_{n+1} + \mathbf{p}_n) - \mathbf{B}_c^T(\tilde{\mathbf{f}}_n^c + \mathbf{f}_n^c)\right]\\ &\quad + \left(\mathbf{M} - \tfrac{h}{2}\mathbf{C} - \tfrac{h^2}{4}\mathbf{K}_b^{\text{global}}\right)\mathbf{v}_n - h\left(\mathbf{K}_b^{\text{global}}\mathbf{u}_n + \mathbf{B}_b^T\mathbf{f}_0^b\right)\\ \mathbf{b}_2 &= \boldsymbol{\Psi}_{\text{UNI}}\tilde{\mathbf{f}}_n^c - \mathbf{b}_{\text{UNI}}\end{aligned} \tag{7b}$$

In the next section, the system of Eqs. (7) is cast in the form of a complementarity problem.

4. Mixed Complementarity Problem (MCP)

The computation of the velocities and slacks at time $n+1$ described by (a) the equation and inequality in (7a), and (b) the complementarity conditions in (5), can be cast into a complementarity problem. First we define the matrix

$$\mathcal{M} = \left[\begin{array}{c|c} \overline{\mathbf{M}} & -\tfrac{h}{2}\mathbf{B}_c^T\mathbf{K}_c\boldsymbol{\Psi}_{\text{UNI}}^T \\ \hline -\tfrac{h}{2}\boldsymbol{\Psi}_{\text{UNI}}\mathbf{K}_c\mathbf{B}_c & \boldsymbol{\Psi}_{\text{UNI}}\mathbf{K}_c\boldsymbol{\Psi}_{\text{UNI}}^T \end{array}\right] \tag{8}$$

and the vectors

$$\mathbf{b} = \left(\mathbf{b}_1^T, \mathbf{b}_2^T\right)^T, \quad \mathbf{q} = -\mathbf{b} \tag{9}$$

Then the problem of computing the velocities and slacks can be stated as

$$\mathcal{M}\begin{pmatrix}\mathbf{v}\\ \boldsymbol{\pi}\end{pmatrix} + \mathbf{q} = \begin{pmatrix}0\\ \mathbf{w}\end{pmatrix} \quad \boldsymbol{\pi} \geqslant 0, \quad \mathbf{w} \geqslant 0, \quad \boldsymbol{\pi}^T\mathbf{w} = 0 \tag{10}$$

The system (10) is a special case of a "Mixed Complementarity Problem" (MCP) [30,20]. The MCP may be solved using a general purpose solver such as the PATH solver [30,31]. However, computational efficiencies can be gained by customizing some linear algebra calculations to take advantage of the special form of the matrix $\mathcal{M}$ that arises in structural mechanics problems. In particular, a Complementary Pivot Algorithm (CPA) is presented in reference [20]

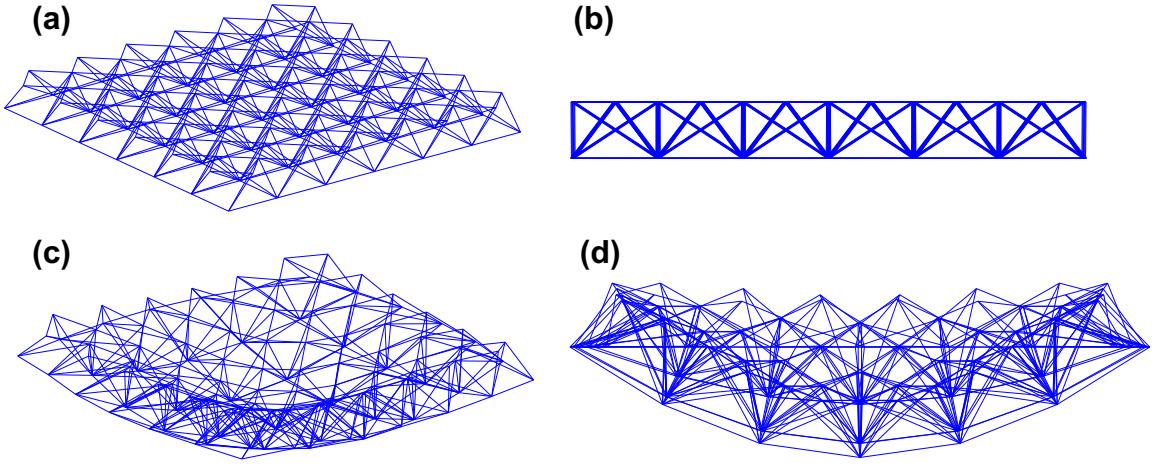

Fig. 8. Example 2 – (a) Isometric view of undeformed shape. (b) Front view of undeformed shape. (c) Isometric view of first mode (frequency, f_1 = 12.7185 Hz) (d) Front view of first mode.

Table 4
Example 2 – Free vibration analysis cases.

Case	Initial configuration	Increment(s)	Result plot
1	First mode shape with no slack cables (Fig. 8)	0.001	Fig. 9
2	Displaced configuration with 24 slack cables (Fig. 10)	0.001	Fig. 11
3	Displaced configuration with 24 slack cables (Fig. 10)	0.01	Fig. 12
4	Displaced configuration with 12 slack cables	0.01, 0.005, 0.001, 0.0005	Fig. 13

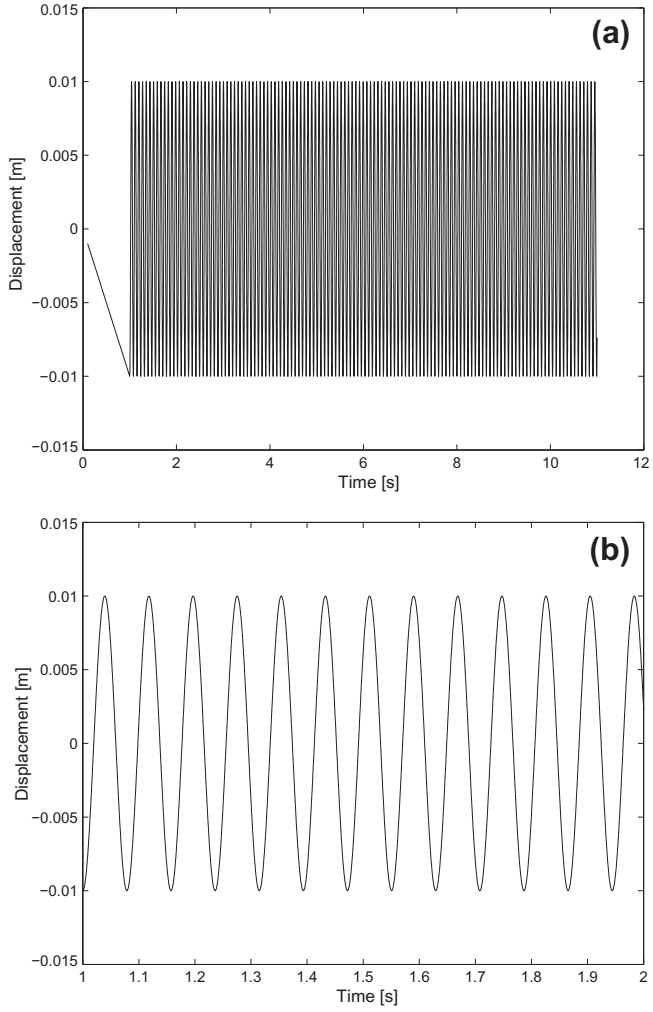

Fig. 9. Example 2 – Free vibration response starting from a deformed configuration corresponding to the first mode with no slack cables. The dynamic response is computed using time step 0.001 s. (a) Displacement of the center node over 10 s of oscillation; the initial displacement for the dynamic phase is imposed quasi-statically over the first 1 s. (b) Zoom-in of the first 1 s of oscillation of the center node.

that uses such linear algebra customizations. In one of the numerical examples that follow, the computational efficiency gained from the linear algebra customization is highlighted. By transforming the MCP of Eq. (10) to a standard LCP (see [32]), it can be shown that it has a unique solution. Thus the problem in each time increment has a unique solution.

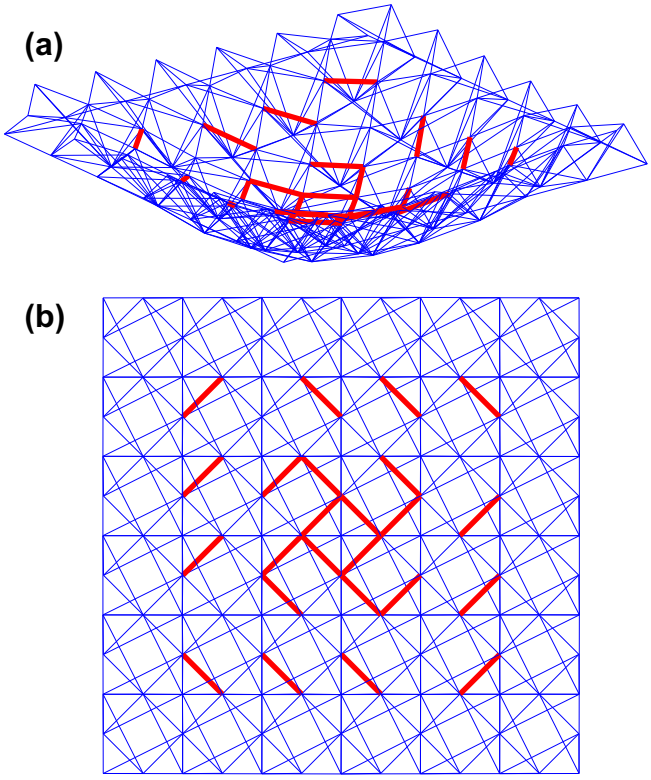

Fig. 10. Example 2 – Deformed configuration with 24 slack cables shown as thick (red) lines. (a) Isometric view. (b) Plan view. (For interpretation of the references to colour in this figure legend, the reader is referred to the web version of this article.)

The computations in each time increment are summarized in Procedure 1.

Procedure 1. Computations in each time increment

1: Compute $\tilde{\mathbf{f}}^c_n$ by the first of Eq. (6) ▷ Predictor computed for each cable
2: Compute $\mathbf{b}_1$ by the first of Eq. (7b) ▷ Global vector assembly
3: Compute $\mathbf{b}_2$ by the second of equations (7b) ▷ Computed for each cable
4: Obtain $\mathbf{v}_{n+1}$ and $\boldsymbol{\pi}_{n+1}$ by solving the complementarity problem (10)
5: Compute $\mathbf{f}^c_{n+1}$ by the second of Eq. (6) ▷ Corrector computed for each cable
6: Compute $\mathbf{u}_{n+1} = \mathbf{u}_n + (h/2)(\mathbf{v}_{n+1} + \mathbf{v}_n)$

4.1. Relationship to existing literature

The conditions in (7a) are obtained by solving the second of Eqs. (5), namely the deformation compatibility equation, for the cable forces $\mathbf{f}^c_{n+1}$, and substituting it into the first of Eq. (5), namely the momentum conservation equation, and into the complementarity condition (using the predictor–corrector format (6)). This results in a *Mixed* Complementarity Problem, mixed since the velocity does not have a $\geqslant 0$ constraint [30]; in fact, it does not have any bound constraints. If instead the reverse is done, i.e., the momentum conservation equation is solved for the velocities $\mathbf{v}_{n+1}$, and this is substituted into the deformation compatibility equation, a Linear Complementarity Problem (LCP) in standard form is obtained,

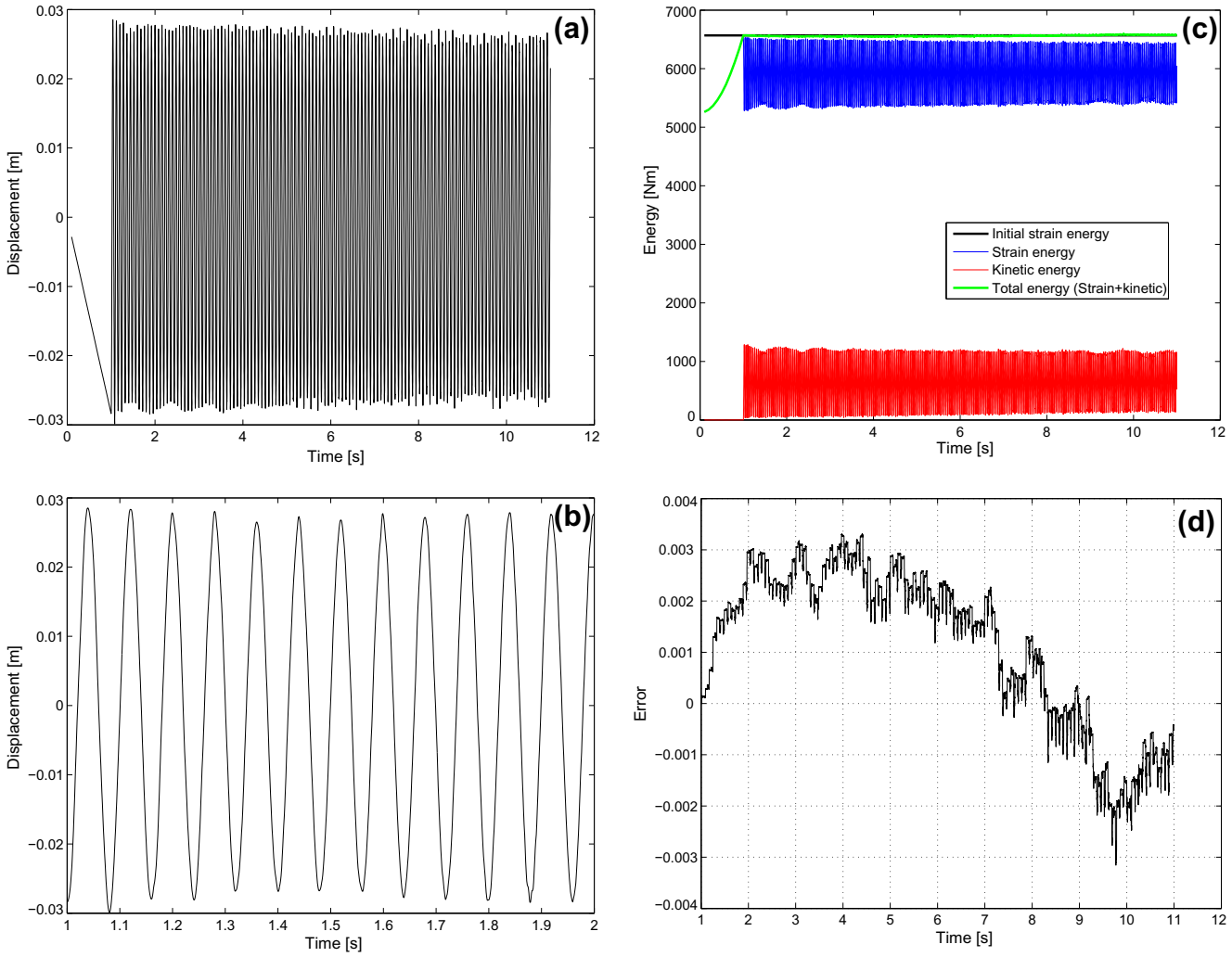

Fig. 11. Example 2 – Free vibration response starting from a deformed configuration with 24 slack cables computed using time step 0.001 s. (a) Displacement of the center node over 10 s of oscillation; the initial displacement for the dynamic phase is applied quasi-statically over the first 1 s. (b) Zoom-in of the first 1 s of oscillation of the center node. (c) Energy balance. (d) Energy error as defined in Eq. (11).

where all the variables, namely the cable slacks, are constrained to be $\geqslant 0$. This latter standard LCP is similar to the formulation presented in [19]. The matrix that arises in this standard LCP when $\boldsymbol{\Psi}_{\text{UNI}} = -\text{Identity}$ is

$$\mathbf{K}_c - \mathbf{K}_c\mathbf{B}_c\overline{\mathbf{M}}^{-1}\mathbf{B}_c^T\mathbf{K}_c$$

the Schur complement of $\mathcal{M}$ in (8) with respect to $\overline{\mathbf{M}}$. When the mass and damping matrix are ignored (statics), this is identical to the matrix in [19]. Unlike the matrix $\overline{\mathbf{M}}$ which has the same sparse structure as the stiffness matrix, the matrix $\mathbf{B}_c\overline{\mathbf{M}}^{-1}\mathbf{B}_c^T$ that appears in the standard LCP does not have a sparse structure. The sparse structure can be utilized to devise efficient computations to solve the MCP (10) [20]. Nineb et.al. [19] develop a domain decomposition approach for large-scale nonsmooth problems. The algorithm used to solve the MCP (10) can be used in the "local stage" of such a domain decomposition approach. The MCP (10) constitutes the Karush–Kuhn–Tucker (KKT) conditions of a Quadratic Program (QP) in $\mathbf{v}$ and $\boldsymbol{\pi}$. This fact can be used for example to compute the necessary derivatives (tangent operator) in the context a domain decomposition approach. The standard form LCP described above constitutes the KKT conditions of a QP in $\boldsymbol{\pi}$ alone.

5. Numerical examples

In this section some numerical examples are presented to illustrate the proposed approach. In particular, two tensegrity structures are considered, both made of the same kind of elementary modules, but different in size, boundary conditions, method of assembly, prestresses, and loading conditions. For the first structure, a series of static analyses are performed, and the results are compared to those presented in the literature [19]. Furthermore, the computational efficiency gained by the linear algebra customizations of the Complementary Pivot Algorithm (CPA) of reference [20] is pointed out. The second structure considered is subjected to a set of dynamic analyses in free vibration and under harmonic loading. Energy balance plots are presented as a means of evaluating the performance of the algorithm and the accuracy of the results.

5.1. Example 1

As a first step in evaluating the performance and reliability of the approach described in the previous sections, the tensegrity grid considered by Nineb et.al. [19] is analyzed. This example has been

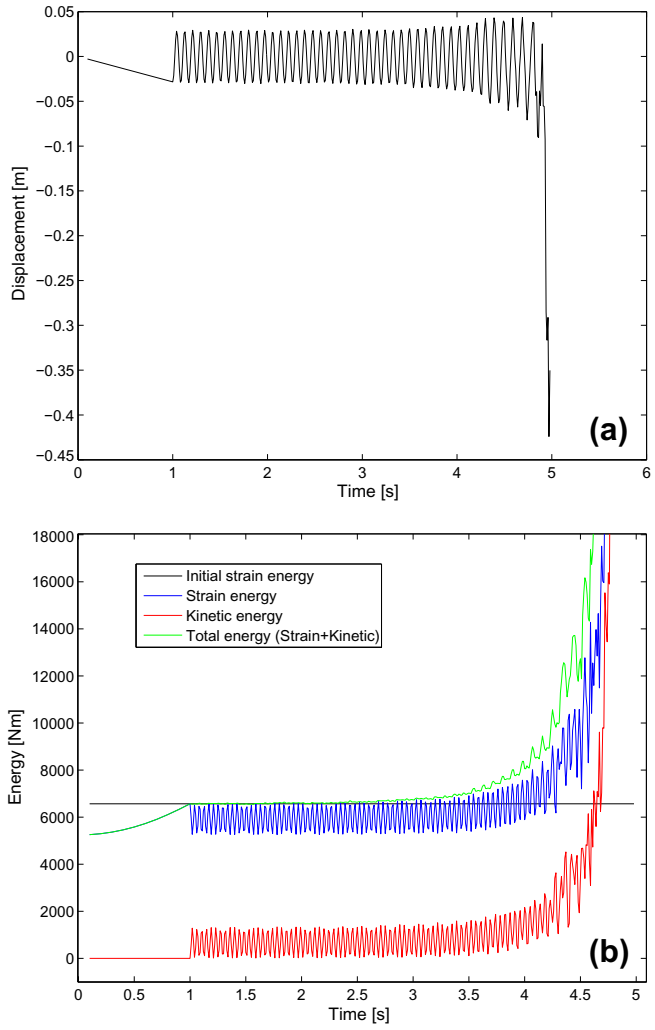

Fig. 12. Example 2 – Free vibration response starting from a deformed configuration with 24 slack cables computed using time step 0.01 s. (a) Displacement of the center node. (b) Energy balance.

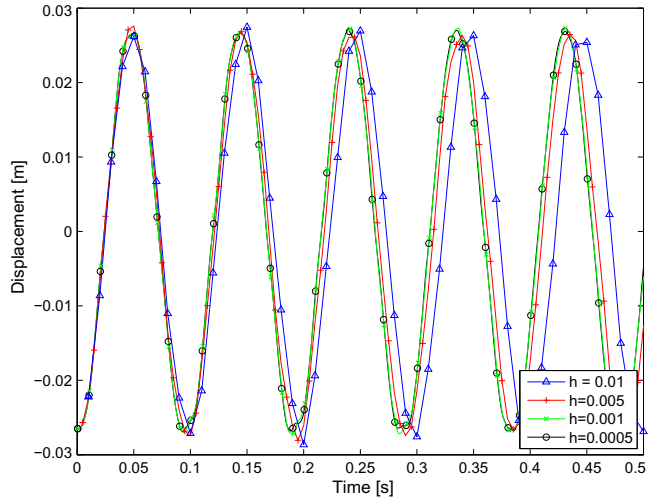

Fig. 13. Example 2 – Convergence of displacement of the center node with decreasing time step size for free vibration starting from a deformed configuration with 12 slack cables.

chosen so that numerical results can be verified against those presented in reference [19]. The example is not intended to represent a typical design. This grid was obtained by duplication of single 8-node self stressed modules [33], shown in Fig. 2 (the sides of the squares in the lower side of the grid thus have two overlapping members, one from each adjacent module, between each pair of nodes). Each module consists of 12 cables and 4 bars. The properties of the elements composing the tensegrity structure are the same as in reference [19], and are summarized in Table 1. The elementary modules are placed one next to the other to form a 16×16 self-stressed tensegrity grid consisting of 833 nodes, 3072 cables and 1024 bars. The assembled structure in its undeformed configuration is shown in Fig. 3. All the lower nodes on two opposite edges of the grid are clamped, and every node is subjected to a vertical static load αp, where p is taken equal to 40 N, and different values of the load factor α are considered in the range from 0 to 1. When $\alpha = 1$, the structure assumes the deformed configuration shown in Fig. 4. Fig. 5(a) shows the tension force in each of the 3072 cables, sorted in increasing order, for different values of the load factor α. Fig. 5(b) shows how the number of slack cables in the structure increases as α is increased from 0 to 1. When $\alpha = 0$, the structure is in its self stressed configuration, and the forces in the cables are simply equal to the initial prestresses. As α increases from 0 to 1, the number of slack cables increases, and for $\alpha = 1$, 13.28% of all cables are slack. The initial prestress configuration and the loads applied are such that several cables slacken around the same level of load between $\alpha = 0.5$ and $\alpha = 0.75$. Based on (i) the norm of the difference between the equilibrium matrices computed in the deformed and undeformed configurations, (ii) the differences between strains computed using various nonlinear measures, and (iii) the size of the geometric stiffness compared to the material stiffness, we find that the use of the small-displacement assumption is justified for this problem. The graphs in Figs. 5(a) and (b) obtained using the PATH solver and the Complementary Pivot Algorithm (CPA) are identical to each other, and appear to be exactly the same as those presented in reference [19].

We next explore the computational efficiency gained by the linear algebra customizations specific to structural mechanics problems utilized in the CPA of reference [20]. This is done by setting the options for the PATH solver as shown in Table 2 to emulate the CPA. The PATH solver however does not utilize the linear algebra customizations. In Fig. 6, the computational times of the CPA are plotted against the number of factorization updates. The computational time required by PATH is 6.16 s as indicated by the dashed line in Fig. 6. The least computational time of 1.44 s is seen to be obtained when the CPA uses 20 factorization updates. The linear algebra customizations thus result in a speedup of about 4.28 for this problem.

5.2. Example 2

The second example is a 6×6 tensegrity grid designed by Quirant et.al. [33]. The elementary modules comprising the grid are of the same kind as the ones in the previous example, but different in size, properties and prestresses. Moreover, the modules are assembled in such a way that they share the cables connecting them to the adjacent modules. The grid consists of 133 nodes, 372 cables and 144 bars. As boundary conditions, the four lower corner nodes are clamped while all the other nodes along the four edges are restrained vertically but free to move in the other directions. The properties of the elements composing the tensegrity structure are as presented by Quirant et.al. [33], and are summarized in Table 3. The assembled structure in its undeformed configuration is shown in Fig. 7. The structure is modeled with a lumped mass matrix, and as having no inherent viscous damping.

First the frequencies and modes of the linearized model are computed. Isometric and front views of the structure in its first mode shape, and in its undeformed configuration are shown in

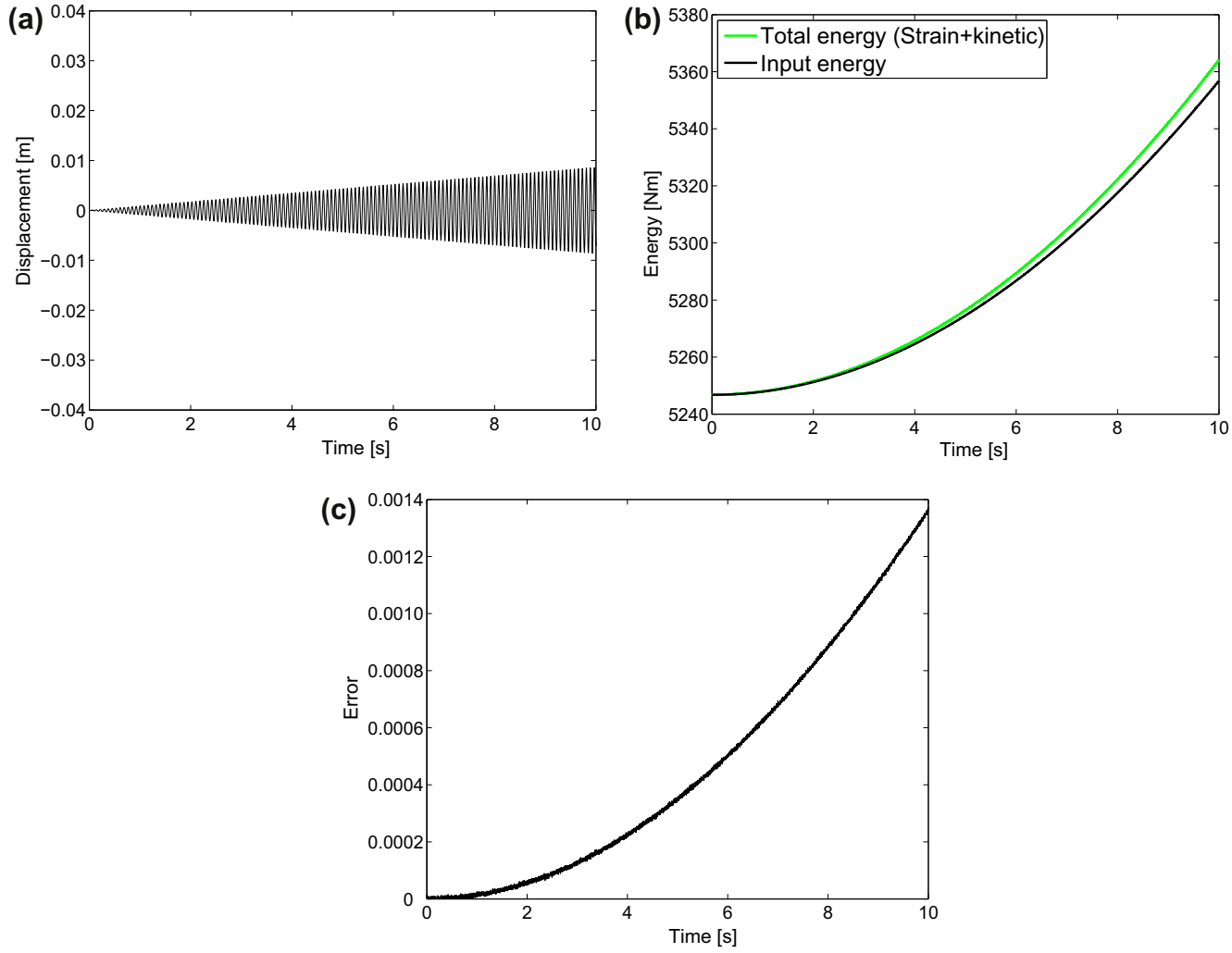

Fig. 14. Example 2 – Forced vibration with input acceleration amplitude 0.01 g, computed using time step 0.001 s. (a) Displacement of center node. (b) Energy balance. (c) Energy error as defined in Eq. (13).

Fig. 8. The first 6 natural frequencies of the linearized model of the tensegrity grid are $f_1 = 12.7185$ Hz, $f_2 = f_3 = 15.2907$ Hz, $f_4 = 21.2673$ Hz, and $f_5 = f_6 = 28.2729$ Hz.

5.2.1. Free vibration analysis

Free vibration analyses of the tensegrity structure are performed starting from different initial configurations as summarized in Table 4.

Case 1: First the structure is displaced into the shape of the first mode of the linearized model without slack cables, and then released. The resulting response, as would be expected, is simple harmonic as seen from the displacement of the center node in Fig. 9.

Case 2: Next, the structure is displaced into the configuration shown in Fig. 10 with 24 slack cables, and then released. The analysis is performed with time increment 0.001 s ($\sim \frac{1}{80}$ of the first mode period of the linearized model). The computed response is shown in Fig. 11. Figs. 11(a) and (b) show the displacement of the center node. In order to evaluate the accuracy of the proposed approach, the total energy is computed. The system is modeled as undamped, and the slackening and tightening of the cables are not associated with energy dissipation. So the total energy of the system, the sum of the strain and kinetic energies must remain constant, and equal to the strain energy in the deformed configuration from which it is released. This energy balance is shown in Fig. 11(a). The energy error defined as

$$\text{energy error} = \frac{\text{total energy} - \text{initial strain energy}}{\text{initial strain energy}} \tag{11}$$

is shown in Fig. 11(b). It is remarkable that despite the non-smooth nature of slackening and tightening of the cables, the relatively large time increment used, and the long duration of the analysis, the largest energy error is only of the order of 0.003. It will be seen later that similarly good long-term energy behavior is obtained in forced vibration analysis as well. This energy balance feature may be attributable to the loose relationship of the time discretization in Section 3 to the notion of Variational Integrators [34]. Further exploration of this relationship is a topic of current work.

Case 3: Although excellent behavior in terms of energy conservation is observed for fairly large time increments, the time increment cannot be arbitrarily large. In this analysis case, the same initial configuration is considered as in case 2. However, a time increment of 0.01 s is used for dynamic analysis. The resulting computation is not stable as seen in Fig. 12.

Case 4: In this analysis case, the goal is to explore convergence of the computed solutions with decreasing time increment. For this, the model is released from an initial configuration with 12

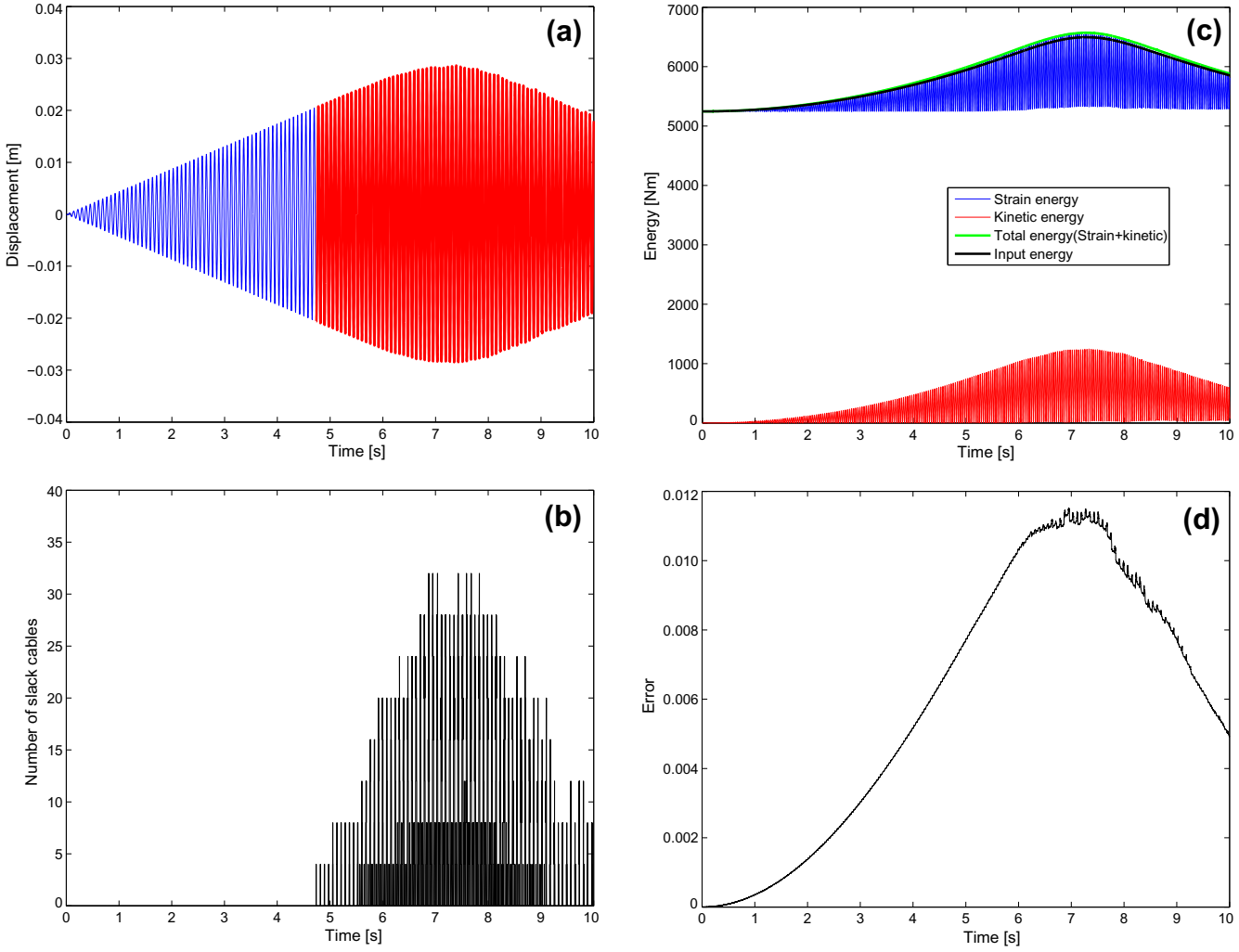

Fig. 15. Example 2 – Forced vibration with input acceleration amplitude 0.05 g, computed using time step 0.001 s. (a) Displacement of the center node with the phase where some cables could be slack is shown in red. (b) Number of slack cables. (c) Energy balance. (d) Energy error as defined in Eq. (13). (For interpretation of the references to colour in this figure legend, the reader is referred to the web version of this article.)

slack cables, and dynamic analysis is performed with four time increments. Fig. 13 indicates convergence of the center node displacement.

5.2.2. Forced vibration analysis with harmonic input

Another set of analyses is performed with harmonic vertical base motion input. The base input acceleration is of the form

$$\ddot{u}_g(t) = \ddot{u}_{g0}\sin(2\pi f_1 t) \tag{12}$$

where $\ddot{u}_{g0}$ is the amplitude of the base acceleration, and $f_1 = 12.7185$ Hz is the frequency of the first mode of the linearized model. Three analysis cases are considered with increasing amplitudes of the input base acceleration. In each case, the dynamic analysis is performed with time increment 0.001 s.

Case 1 ($\ddot{u}_{g0} = 0.01$ g): The computed response is shown in Fig. 14. No cables slacken in the first 10 s, and the displacement of the center node seen in Fig. 14(a) shows the characteristic linear growth of resonance. We again explore the long-term energy balance. Unlike in the free vibration case, the input energy needs to be taken into account when considering energy balance. The input energy is computed as

$$\text{input energy}(t) = \int_0^t \sum R_s(\tau)v_s(\tau)\mathrm{d}\tau$$

where R_s and v_s are the reactions and velocities of the supports at the base. The energy error in the forced vibration case is defined as

$$\text{energy error} = \frac{\text{total energy} - \text{input energy}}{\text{input energy}} \tag{13}$$

The total and input energies are shown in Fig. 14(b), and the energy error in Fig. 14(c).

Case 2 ($\ddot{u}_{g0} = 0.05$ g): The displacement of the center node of the grid in shown in Fig. 15(a). Just before 5 s, when the amplitude of the response is about 0.02 m, some cables become slack. The phase of motion where a number of cables in the structure go from being in tension to being slack and vice versa is indicated in red in Fig. 15(a). The number of slack cables at each instant of time is plotted in Fig. 15(b). The energy balance and the error are shown in Figs. 15(a) and (b) respectively. The largest error is seen to be smaller than 0.012.

Case 3 ($\ddot{u}_{g0} = 0.1$ g): The displacement of the center node of the grid in shown in Fig. 16(a). As in Case 2, cables start to become slack when the amplitude of this displacement is about 0.02 m,

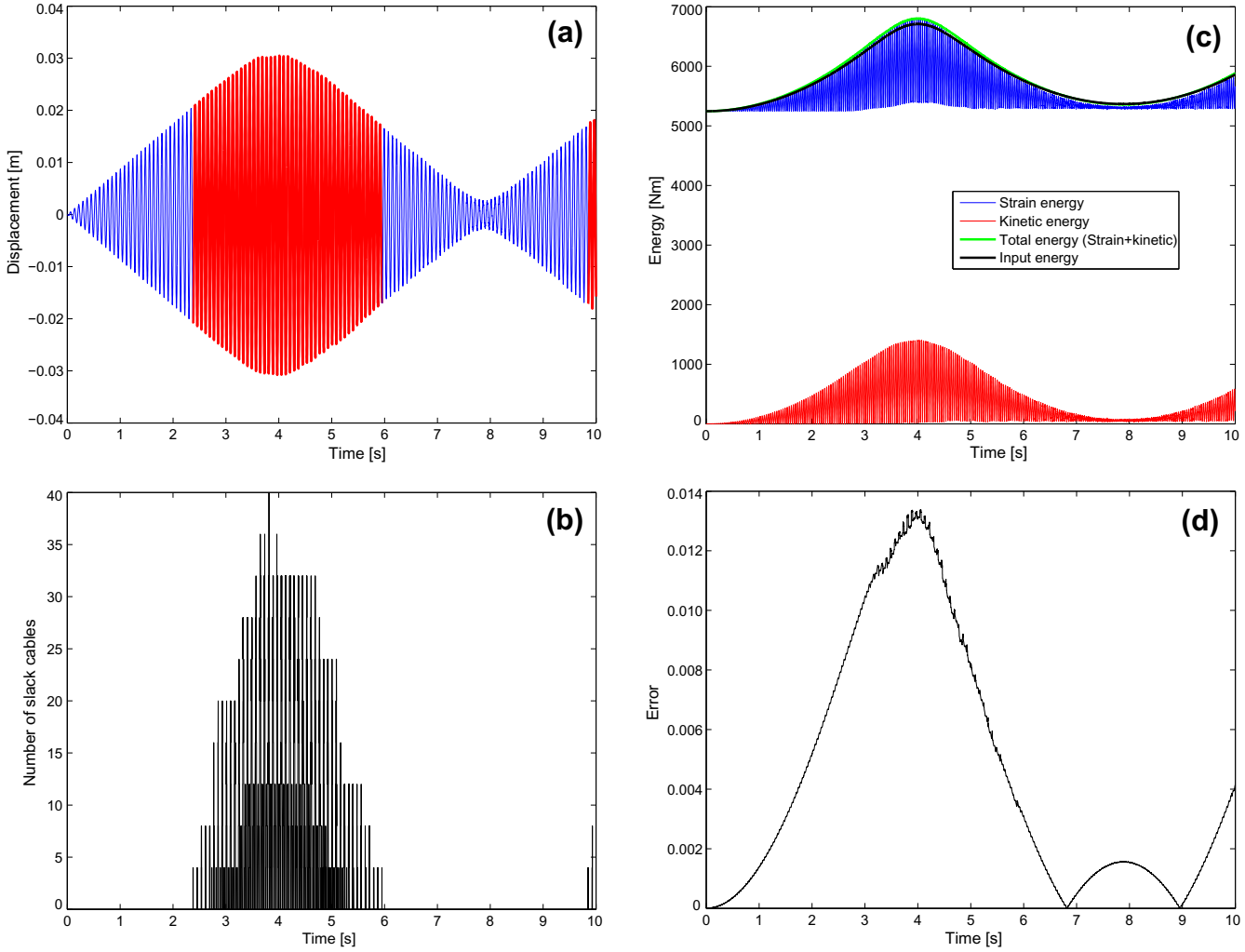

Fig. 16. Example 2 – Forced vibration with input acceleration amplitude 0.1 g, computed using time step 0.001 s. (a) Displacement of the center node with the phase where some cables could be slack is shown in red. (b) Number of slack cables. (c) Energy balance. (d) Energy error as defined in Eq. (13). (For interpretation of the references to colour in this figure legend, the reader is referred to the web version of this article.)

but this occurs at earlier time than in Case 2. The number of slack cables against time is shown in Fig. 16(b). The energy balance and energy are plotted in Figs. 16(a) and (b). The largest error in this case is smaller than 0.014.

Thus excellent long-term energy balance is observed in forced vibration analysis as well.

6. Concluding remarks

An approach has been presented for the dynamic analysis of tensegrity structures. It is based on casting the computation in each time increment as a complementarity problem. Numerical examples illustrate the excellent long-term energy balance of the computed solutions. In addition, significant computational efficiency can be gained by linear algebra customizations in solving the complementarity problem. As discussed in Section 2.1, due to the use of linear kinematics the above method is not applicable to tensegrity structures with internal mechanisms or where geometric stiffness is significant compared to material stiffness. A large displacement formulation based on complementarity is a topic of current work.

Acknowledgements

The first author's visit to the University of Colorado was made possible through a grant from the Clifford C. Furnas Chair at the University at Buffalo. The second author gratefully acknowledges financial support from the National Science Foundation through the Grant CMMI-0847053. The authors wish to thank Andrei M. Reinhorn, Clifford C. Furnas Eminent Professor at the University at Buffalo, for enabling their collaboration. The authors also acknowledge the anonymous reviewers for their valuable comments related to implications for large-displacement analyses.

References

[1] Tibert AG, Pellegrino S. Review of form-finding methods for tensegrity structures. Int J Space Struct 2003;18(4):209–23.
[2] Zhang L, Maurin B, Motro R. Form-finding of nonregular tensegrity systems. J Struct Eng 2006;132(9):1435–40.
[3] Rieffel J, Valero-Cuevas F, Lipson H. Automated discovery and optimization of large irregular tensegrity structures. Comput Struct 2009;87(5–6):368–79.
[4] Calladine CR. Buckminster Fuller's 'Tensegrity' structures and Clerk Maxwell's rules for the construction of stiff frames. Int J Solids Struct 1978;14(2):161–72.
[5] Pellegrino S, Calladine CR. Matrix analysis of statically and kinematically indeterminate frameworks. Int J Solids Struct 1986;22(4):409–28.

[6] Sultan C. Tensegrity: 60 years of art, science, and engineering. In: Aref H, Giessen Evd, editors. Advances in applied mechanics, advances in applied mechanics, vol. 43. Elsevier; 2009. p. 69–145.
[7] Sultan C, Corless M, Skelton RE. Peak to peak control of an adaptive tensegrity space telescope. In: Proceedings of the SPIE-the international society for optical engineering, vol. 3667, 1999, pp. 190–201.
[8] Sultan C, Corless M, Skelton RE. Tensegrity flight simulator. J Guid Control Dyn 2000;23(6):1055–64.
[9] Tibert AG, Pellegrino S. Deployable tensegrity reflectors for small satellites. J Spacecraft Rockets 2002;39(5):701–9.
[10] Ingber DE. The architecture of life. Sci Am 1998;278(1):48–57.
[11] Yaozhi L, Xian X, Lele T, Kumar S, Ingber DE. A multi-modular tensegrity model of an actin stress fiber. J Biomech 2008;41(11):2379–87.
[12] Stamenovic D, Wang N, Ingber DE. Cellular tensegrity models and cell-substrate interactions. In: King MR, editor. Principles of cellular engineering. Academic Press; 2006. p. 81–104.
[13] Aldrich JB, Skelton RE, Kreutz-Delgado K. Control synthesis for a class of light and agile robotic tensegrity structures. Proceedings of the 2003 American control conference. Piscataway, NJ, USA: IEEE; 2003. p. 5245–51.
[14] Shibata M, Saijyo F, Hirai S. Crawling by body deformation of tensegrity structure robots. 2009 IEEE International conference on robotics and automation (ICRA). Piscataway, NJ, USA: IEEE; 2009. p. 4375–80.
[15] Juan SH, Skelton RE, Mirats Tur JM. Dynamically stable collision avoidance for tensegrity based robots. Proceedings of the 2009 ASME/IFToMM international conference on reconfigurable mechanisms and robots, ReMAR 2009. London, United kingdom: IEEE Computer Society; 2009. p. 315–22.
[16] Skelton RE, de Oliveira MC. Tensegrity systems. Dordrecht; New York: Springer; 2009.
[17] Juan SH, Tur JMM. Tensegrity frameworks: static analysis review. Mech Mach Theory 2008;43(7):859–81.
[18] Tur JMM, Juan SH. Tensegrity frameworks: dynamic analysis review and open problems. Mech Mach Theory 2009;44(1):1–18.
[19] Nineb S, Alart P, Dureisseix D. Domain decomposition approach for non-smooth discrete problems, example of a tensegrity structure. Comput Struct 2007;85(9):499–511.
[20] Sivaselvan MV. Complementarity framework for nonlinear dynamic analysis of skeletal structures with softening plastic hinges. Int J Numer Methods Eng 2010;86(2):182–223.
[21] Maier G. A matrix structural theory of piecewise linear elastoplasticity with interacting yield planes. Meccanica 1970;5(1):54–66.
[22] Acary V, Brogliato B. Numerical methods for nonsmooth dynamical systems: applications in mechanics and electronics. Berlin: Springer; 2008.
[23] Pellegrino S. Analysis of prestressed mechanisms. Int J Solids Struct 1990;26(12):1329–50.
[24] Calladine CR, Pellegrino S. First-order infinitesimal mechanisms. Int J Solids Struct 1991;27(4):505–15.
[25] Calladine CR, Pellegrino S. Further remarks on first-order infinitesimal mechanisms. Int J Solids Struct 1992;29(17):2119–22.
[26] Guest S. The stiffness of prestressed frameworks: a unifying approach. Int J Solids Struct 2006;43(3–4):842–54.
[27] Sivaselvan MV, Reinhorn AM. Lagrangian approach to structural collapse simulation. J Eng Mech – ASCE 2006;132(8):795–805.
[28] Sivaselvan MV, Lavan O, Dargush GF, Kurino H, Hyodo Y, Fukuda R, et al. Numerical collapse simulation of large-scale structural systems using an optimization-based algorithm. Earthquake Eng Struct Dyn 2009;38(5):655–77.
[29] Chopra AK. Dynamics of structures: theory and applications to earthquake engineering. 3rd ed. Upper Saddle River, N.J.: Pearson/Prentice Hall; 2007.
[30] Dirkse SP, Ferris MC. The PATH solver: a non-monotone stabilization scheme for mixed complementarity problems. Optim Methods Softw 1995;5:123–56.
[31] Munson T.S. Algorithms and Environments for Complementarity, Ph.D. thesis, University of Wisconsin–Madison, 2000.
[32] Cottle R, Pang J-S, Stone RE. The linear complementarity problem. Boston: Academic Press; 1992.
[33] Quirant J, Kazi-Aoual MN, Motro R. Designing tensegrity systems: the case of a double layer grid. Eng Struct 2003;25(9):1121–30.
[34] Fetecau RC, Marsden JE, Ortiz M, West M. Nonsmooth lagrangian mechanics and variational collision integrators. SIAM J Appl Dyn Syst 2003;2:381–416.